AGU PUBLICATIONS

Geophysical Research Letters

RESEARCH LETTER
10.1002/2014GL060832

Key Points:
- Observational iceberg data from 2012 Baffin Bay field experiment
- Mathematical model of iceberg decay due to hydrostatic stresses
- Analytic expressions for iceberg profiles and breakup conditions developed

Supporting Information:
- Supplemental Figures S1–S3

Correspondence to:
T. J. W. Wagner,
tjwagner@ucsd.edu

Citation:
Wagner, T. J. W., P. Wadhams, R. Bates, P. Elosegui, A. Stern, D. Vella, E. Povl Abrahamsen, A. Crawford, and K. W. Nicholls (2014), The "footloose" mechanism: Iceberg decay from hydrostatic stresses, *Geophys. Res. Lett.*, *41*, 5522–5529, doi:10.1002/2014GL060832.

Received 9 JUN 2014
Accepted 11 JUL 2014
Accepted article online 15 JUL 2014
Published online 7 AUG 2014

The "footloose" mechanism: Iceberg decay from hydrostatic stresses

Till J. W. Wagner[1,2], Peter Wadhams[2], Richard Bates[3], Pedro Elosegui[4], Alon Stern[5], Dominic Vella[6], E. Povl Abrahamsen[7], Anna Crawford[8], and Keith W. Nicholls[7]

[1]Scripps Institution of Oceanography, University of California, San Diego, La Jolla, California, USA, [2]Department of Applied Mathematics and Theoretical Physics, University of Cambridge, Cambridge, UK, [3]School of Geography and Geosciences, University of St. Andrews, Saint Andrews, UK, [4]Institute of Marine Sciences, CSIC, Barcelona, Spain, [5]Courant Institute of Mathematical Sciences, New York University, New York, New York, USA, [6]Mathematical Institute, University of Oxford, Oxford, UK, [7]British Antarctic Survey, NERC, Cambridge, UK, [8]Department of Geography and Environmental Studies, Carleton University, Ottawa, Ontario, Canada

Abstract We study a mechanism of iceberg breakup that may act together with the recognized melt and wave-induced decay processes. Our proposal is based on observations from a recent field experiment on a large ice island in Baffin Bay, East Canada. We observed that successive collapses of the overburden from above an unsupported wavecut at the iceberg waterline created a submerged foot fringing the berg. The buoyancy stresses induced by such a foot may be sufficient to cause moderate-sized bergs to break off from the main berg. A mathematical model is developed to test the feasibility of this mechanism. The results suggest that once the foot reaches a critical length, the induced stresses are sufficient to cause calving. The theoretically predicted maximum stable foot length compares well to the data collected in situ. Further, the model provides analytical expressions for the previously observed "rampart-moat" iceberg surface profiles.

1. Introduction

The collapse of large ice shelves in Antarctica and the accelerated calving of glaciers in Greenland and Ellesmere Island in recent years have led to an increased volume of icebergs in both polar regions [*Rignot et al.*, 2004; *Alley*, 2005; *Derksen et al.*, 2012]. At the same time, there has been a rapid rise in commercial interest in these regions. This has been particularly the case for the Arctic where the retreat of summer sea ice has opened new shipping routes [*Smith and Stephenson*, 2013] and rekindled the idea of profitable extraction of oil and gas [*McClintock*, 2011]. However, icebergs still pose a major threat to ships and offshore structures, and so the mounting interest in the high latitudes has come with a renewed interest in iceberg trajectories and life cycle—from both observations [e.g., *Martin et al.*, 2010; *Timco*, 2007; *Gladstone et al.*, 2001] and modeling efforts [e.g., *Keghouche and Bertino*, 2009]. Aside from such engineering applications, the deterioration and melting of icebergs (or ice islands, as large tabular icebergs are referred to in the Arctic) is of fundamental interest to oceanographers, since this is a significant contributor to the freshwater flux in the polar seas [*Silva et al.*, 2006]. From a climatological point of view, icebergs are thought to have played a key role in past climatic shifts. In particular, paleoclimatologists have shown that large numbers of icebergs were shed during the last glacial period in the so-called "Heinrich events" [*Sierro et al.*, 2005].

Among the multiple thermodynamic and mechanical processes involved in iceberg decay, forced convection, calving-/wave-induced flexural failure, and wave erosion are commonly taken to be the most important [*Savage*, 2001]. The first is due to differential iceberg-water velocities, the second is purely mechanical, and the third is usually regarded as the most efficient decay factor [*White et al.*, 1980]. Other, less significant contributors to iceberg decay are insolation, buoyant meltwater convection [*Huppert and Turner*, 1978], and wind-forced convection.

Savage [2001] lists three distinct calving mechanisms: (i) flexural breakups due to ocean swell [*Goodman et al.*, 1980; *Wadhams*, 2000], (ii) calving of ice overhangs that result from wave erosion at the waterline [*White et al.*, 1980], and (iii) calving of the buoyant foot that also appears due to wave erosion. It is the third of these that concerns us here. Although it should be considered a significant decay mechanism in its own right (as we argue below), its importance is rarely discussed. An exception to this is the work by *Scambos et al.*

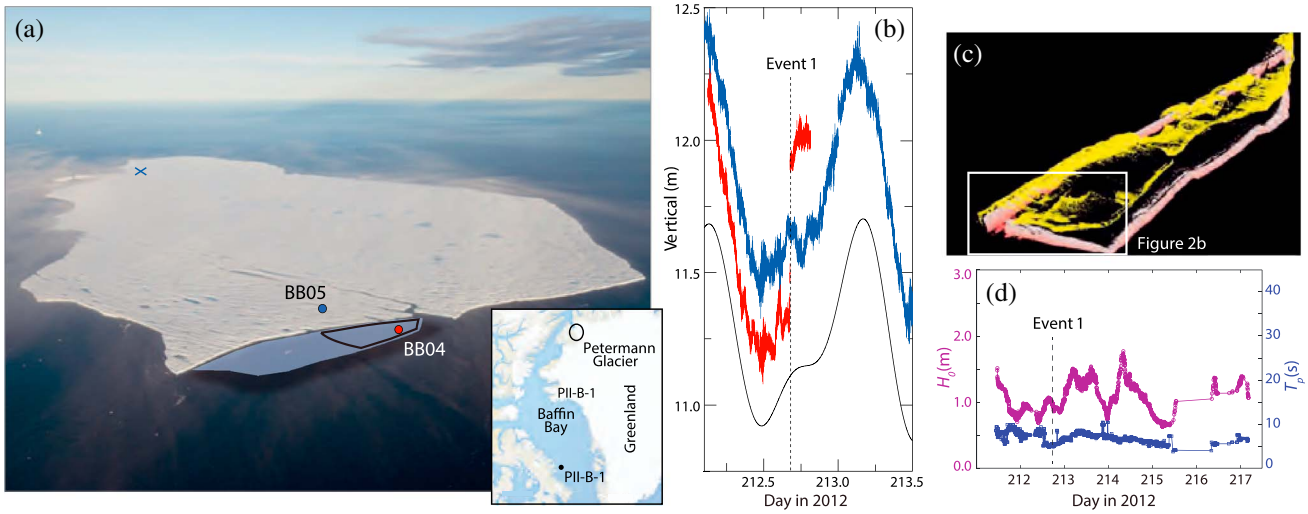

Figure 1. (a) Aerial view of PII-B-1 showing the approximate deployment locations of GPS stations (circles) BB04 (red) and BB05 (blue). For scale, the distance between BB04 and BB05 is ~210 m. The piece of ice on which BB04 is located is drawn to resemble the iceberg geometry prior to breakup. The black outline corresponds roughly to the broken-off piece shown in Figure 1c. The far end of the iceberg was pinned to the seabed during the period of observations, approximately at the point labeled with a cross. (Photo: Chris Packham) Inset: location of PII-B-1 in Baffin Bay (Google Maps); (b) vertical position estimates in the WGS84 ellipsoid. Site color coding as in Figure 1a. Black line: predicted ocean tide using the AOTIM-5 model [*Padman and Erofeeva*, 2004]. The jump in elevation of BB04 at day ~212.7 corresponds to the breakup during Event 1 of the piece of ice shown in blue in Figure 1a; (c) 3-D lidar scan (yellow) and multibeam sonar image (red) of freeboard and keel, respectively, of the shape outlined in black in Figure 1a; (d) data from a "Waverider" buoy located close to the iceberg, collected over the period of the experiment. Shown are significant wave height H_0 (purple circle) and modal period T_p (blue square).

[2005, 2008], who performed observational and modeling studies of "edge wasting" processes—a catch-all term used to describe the combination of mechanisms (i)–(iii) described above. That this process has been largely neglected in the literature may be due to "the lack of quantitative theories [of such a mechanism...]" *Savage* [2001].

In this letter we provide a simple quantitative theory (for idealized geometric, material, and fracture conditions) to fill this gap in our understanding of iceberg decay. Our interest in this phenomenon was initially sparked by a number of large-scale calving events we observed in calm conditions and without significant tidal forcing during a recent field experiment (see section 2). We argue that these events are best explained by flexural breakup due to the torque exerted on the berg by a submerged foot—what we call the "footloose" mechanism. (A more standard term for a submerged fringe around an iceberg is a "ram" [*Armstrong et al.*, 1973; *World Meteorological Organization*, 1970], but we use the term "foot" here as it is more descriptive of a fringe than of a single protuberance).

2. Operation Iceberg Experiment

Despite the substantial interest, icebergs have rarely been studied in situ. This is largely due to such field experiments being difficult and not without inherent dangers: large icebergs are known to create their own local weather, making helicopter transportation to and from an iceberg challenging. More difficult still is the terrain: icebergs are prone to breakup and capsize spontaneously and also present an ideal retreat for polar bears in the Arctic summer. All of these dangers were encountered during the experiment discussed below.

The ice island surveyed during the "Operation Iceberg" experiment as part of a two-episode British Broadcasting Corporation (BBC) documentary was the largest remaining fragment of the ~253 km^2 Petermann Ice Island (PII) that calved from Petermann Glacier, northwest Greenland, in August 2010 [*Falkner et al.*, 2011]. At the time of data collection in late July 2012, PII-B-1, as the surveyed fragment became known, was ~42 km^2 in area with an average thickness of ~70 m. It had then drifted to Baffin Bay and was located 130 km southeast of Clyde River, NU, Canada, where it was grounded at one point and subject to substantial diurnal rotation around that point, caused by tidal forcing. During the experiment, a number of large

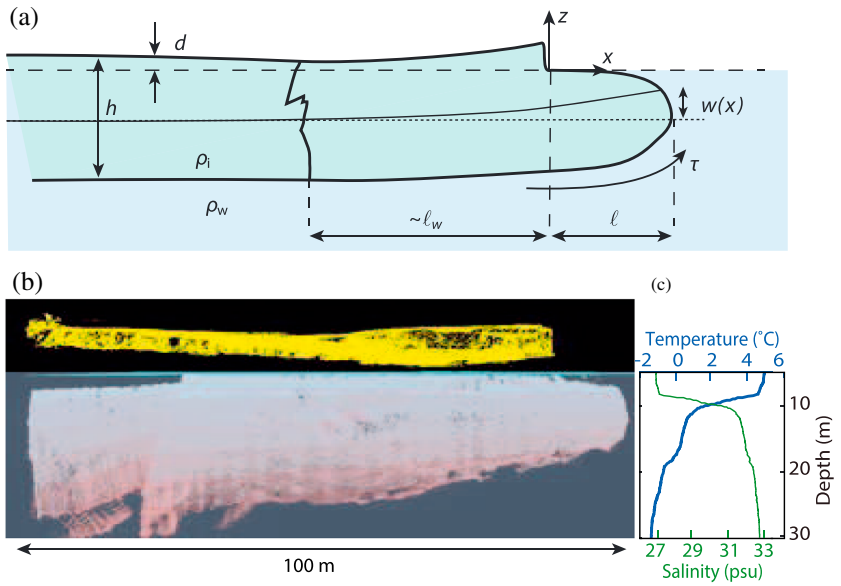

Figure 2. (a) Schematic of an "iceberg beam" of thickness h extending from $-\infty$ to l. The freeboard d is eroded in the region $0 < x < l$, resulting in an underwater foot (see text). The deflection of the centerline of the beam $w(x)$ (solid line) is shown relative to the undeflected state (dotted line). For a large enough torque τ, the iceberg will fracture at $x \simeq -\ell_w$, as indicated. Ice and water density are ρ_i and ρ_w, respectively. (b) "Cross section" of the calved piece from Figure 1c, with lidar scan of the freeboard (yellow) and MB scan of the keel (red). (c) Temperature and salinity profiles for the surface layer next to the iceberg edge, showing that the sea surface layer is strongly stratified with temperatures several degrees above melting (depths aligned with the scan in Figure 2b).

calving events (with broken-off pieces > 100 m in diameter) were observed. The breakup process of one of those events, henceforth "Event 1," was measured by GPS. We occupied a total of five sites on the iceberg surface with geodetic quality GPS-receiving systems for a period of ~5 days, from 30 July to 3 August (days of year 2012/212–216). Two of the systems operated continuously and simultaneously during Event 1, recording observations at least once every 3 s. Prior to breakup, the two systems formed a 209.8 m long baseline. After breakup, one system (BB05) continued operating on the main berg while the second (BB04) rose up and drifted away on the piece that broke off; BB04 was eventually recovered, about 3.2 h after Event 1. Locations of the antennae and estimates of the vertical component of site position in the WGS84 ellipsoid are shown in Figures 1a and 1b, respectively. The least squares estimate of a vertical offset of BB04 relative to BB05 due to breakup is 63.1 ± 0.4 cm. The rise of BB04 suggests that prior to calving, this part of the berg was submerged below its own equilibrium floating depth. A natural explanation is that this submersion was caused by a bending torque exerted by the (thicker) remainder of the berg, which in turn may have initiated or contributed to the breakup.

Also shown on the aerial image is the approximate shape of the total broken-off piece, and the outline of a 3-D scan of one of its subsegments. The scan was obtained using an Optec lidar to measure the freeboard of the iceberg edge and a Reson 8125 multibeam sonar (MB) to measure its keel. Rendered images of the scan are shown in Figures 1c and 2b. Lidar/MB surveys were performed throughout the experiment, resulting in 3-D scans of the complete iceberg perimeter. From the scans it emerges that almost the entire edge of the berg features a protruding underwater foot as shown in Figure 2. The foot was on average ~19 m wide and less than ~61 m thick (this value is an upper bound, estimated from freeboard data, since the full thickness was not visible to the MB). The observation of this foot and the vertical leap of the broken-off piece led to the suggestion of the "footloose mechanism," which we develop below.

We believe that the observed calvings may not have been due to wave action, although this still remains a possibility because the iceberg was thin and weak compared with thicker Antarctic tabular icebergs which have been shown to require a significant swell to break up [*Wadhams et al.*, 1983]. The data collected from the Waverider buoy show that the iceberg experienced only modest swell conditions during the experiment, with significant wave heights less than 2 m and modal wave period 9–12 s (Figure 1d).

Nevertheless, fracture mechanics considerations [*Goodman et al.*, 1980] show that a weakened iceberg with many crevasses could easily have a crack large enough to propagate at low flexural stress.

We further believe that tidal stresses did not cause the observed calvings because for a berg grounded at a single point, the stress field within the berg due to tidal forcing will be roughly radial around the grounding location. As will become clear from the model in section 3, for an iceberg of thickness ~ 70 m, the bending stress peaks at a distance $\lesssim 250$ m from the point of grounding. Therefore, since PII-B-1 was grounded near its edge, a breakup due to tides would likely result in a small piece of diameter < 500 m remaining grounded and the main iceberg becoming unstuck. Our observations, on the other hand, found pieces calving from the edge farthest from the grounding point (Figure 1a), at a distance at which tidal effects should have largely dissipated (e.g., Event 1 occurred approximately 8 km from the grounding point).

3. The Footloose Mechanism

In summer in Baffin Bay, icebergs quickly find themselves surrounded by open water with surface temperatures far above freezing. A combination of warm surface waters (Figure 2c) and forced convection due to surface waves causes a much higher rate of melting at the waterline of the iceberg than deeper down, resulting in melt rates at the waterline up to 1 m/d/°C [*Scambos et al.*, 2008; *Savage*, 2001]. The result is the appearance of a so-called "wavecut," which is commonly observed for icebergs in relatively warm waters [*Veitch et al.*, 2001]. The propagation of such a wavecut is likely to be further enhanced by calm conditions in which the vertical mixing in the surface water layer is small and the top water layer can heat up easily (e.g., from solar radiation), as illustrated in Figure 2c. Once the wavecut reaches a critical depth, the overhanging freeboard will become unstable and break off [*White et al.*, 1980], leaving behind a protruding underwater ice foot (Figures 1c and 2b). The foot is submerged because it is attached to the main berg; since it is buoyant relative to the surrounding water, it exerts a net vertical force on the berg. This vertical force can have two effects: (i) for smaller icebergs with an asymmetric foot around their edges, the buoyant foot will raise and tilt the iceberg with respect to the waterline [see *Scambos et al.*, 2008, Figures 5g and 5h] and (ii) for large bergs with a significant foot around their edges, the buoyancy induces a net local hydrostatic imbalance. This imbalance in turn results in a deformed edge profile and a corresponding internal stress field which reaches a maximum further inside the iceberg (away from the edge). We propose that this maximum stress can reach a critical level (for a large enough ice foot) that ultimately causes the iceberg to calve. A simplistic model for the special case of an exactly symmetric iceberg was previously discussed in *Diemand* [1987]. Here we present a quantitative model to describe this footloose mechanism for large tabular icebergs in terms of a floating cantilever beam that is subjected to a vertical forcing.

In order to present a simple physical model that captures the essential features of the footloose mechanism proposed above, we make a number of simplifying assumptions. Most notable among these assumptions is that we model the iceberg and its foot as a purely elastic beam with a well-defined breaking, or yield stress σ_y, and a constant Young's modulus E. We therefore neglect the effect of cracks and crevasses, which inevitably weaken the effective "beam." In calculating the deformation of the berg, we also neglect the change in bending stiffness that occurs between the foot and the main berg; we assume that the change in thickness is only important in determining the loading on the beam. Motivated by the rectilinear features of the berg illustrated in Figure 1a, we also neglect variations around the circumference of the berg: our model is two dimensional. With these assumptions the vertical deflection $w(x)$ of the berg from its floating depth satisfies [*Vella and Wettlaufer*, 2008]

$$Bw''''(x) + \rho_w g w(x) = Q(x), \tag{1}$$

where $B = Eh^3/12(1-\nu^2)$ is the bending stiffness of a beam [*Landau and Lifshitz*, 1986] of thickness h and Poisson ratio ν, g is the acceleration due to gravity, and ρ_w the density of water (Figure 2a). In equation (1), the first term represents the restoring force on the beam due to its bending stiffness, the second term accounts for the buoyancy of the displaced water acting on the iceberg, and $Q(x)$ is the additional buoyancy arising from the foot.

The mathematical character of the solutions of equation (1) is well known [*Hetényi and Hetbenyi*, 1946] to be oscillations modulated by an exponential decay over a horizontal length

$$\ell_w = \left(B/g\rho_w\right)^{1/4}. \tag{2}$$

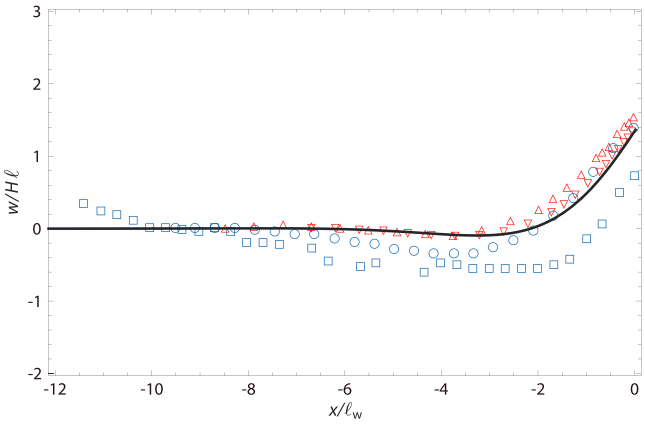

Figure 3. Comparison of the theoretically obtained, dimensionless, deflection $w(x)/(\mathcal{H}\ell)$ (black line) to the nondimensionalized observational data (blue) and finite element method (FEM) (red) model output from *Scambos et al.* [2005], for icebergs A38B (inverted triangle and circle) and A43B (triangle and square); errors are smaller than marker sizes. The height of the natural surface level is chosen to approximately fit the model.

This intrinsic "buoyancy length" reflects the balance of the beam's stiffness and the loading of hydrostatic pressure [*Wagner and Vella*, 2011]. However, the details depend on the precise form of the loading $Q(x)$.

When the length of the ice foot ℓ is relatively short compared to the buoyancy length ℓ_w, i.e., $\ell \ll \ell_w$, the bending of the foot may be neglected and the length of the foot only enters via the total buoyancy force that it imparts on the rest of the beam; the foot may be modeled as a point force acting on the edge of the beam, $Q(x) = F\delta(x)$, where $\delta(x)$ is the Dirac delta function and the total force $F = F_{\text{buoyancy}} - F_{\text{gravity}} = \ell g \rho_i d$, where $d \equiv h\Delta\rho/\rho_w$ is the freeboard of the sheet in isostatic equilibrium, with $\Delta\rho \equiv \rho_w - \rho_i$. Solving (1) subject to moment free and known force boundary conditions at $x = 0$ (the edge of the foot) and undisturbed conditions as $x \to -\infty$, we find that

$$w(x) = \sqrt{2}\mathcal{H}\ell \exp\left(\frac{x}{\sqrt{2}\ell_w}\right)\cos\frac{x}{\sqrt{2}\ell_w}, \tag{3}$$

where $\mathcal{H} \equiv d\rho_i/(\rho_w\ell_w)$ is a scaled, dimensionless thickness of the iceberg that emerges naturally from the calculation. (Further details may be found in SI). This profile is qualitatively similar to the "rampart-moat" morphology observed previously [*Scambos et al.*, 2005], as shown in Figure 3 and discussed in section 4.

To determine conditions under which the loading from the foot may induce breaking, we compute the stress within the beam associated with bending. From plate theory the maximum stress within a beam occurs at the surfaces and is given by $\sigma_{\max} = Y|w''_{\max}| = Y\mathcal{H}\ell/\ell_w^2 \exp(-\pi/4)$ [*Mansfield*, 2005], where $Y = Eh/2(1-\nu^2)$ is the stretching stiffness of a beam of thickness h. Within our simple elastic model, we assume that provided $\sigma_{\max} < \sigma_y$, no fracture occurs and the berg remains intact. Combining this result with (3), we find that a foot with length

$$\ell < \ell_{\text{crit}} = \frac{e^{\frac{\pi}{4}}}{6}\frac{\rho_w}{\rho_i}\frac{h}{\ell_w}\frac{\sigma_y}{g\Delta\rho}, \tag{4}$$

may exist without the berg fracturing. When $\ell = \ell_{\text{crit}}$, the berg will fracture at the point of maximum stress which is found at $x_{\max} = -(\pi/2\sqrt{2})\ell_w$, i.e., roughly at a distance ℓ_w from the edge. We note that (4) would make it possible in principle to estimate the large-scale yield strength (or, alternatively, the elastic modulus) of an iceberg from observations of ℓ_{crit}, for a given material and geometric properties.

We emphasize that the analysis leading to (4) was predicated on the assumption that $\ell \ll \ell_w$; for this approximation to be self-consistent we require $\sigma_y h/(\ell_w^2 g\Delta\rho) \ll 1$. Analytical results may still be obtained once this restriction is lifted, i.e., when $\ell \sim \ell_w$, but the final criterion for the maximum foot length ℓ_{crit} must be determined numerically (for details, see SI). However, an important feature of the calculation is that we find that a natural stress scale exists: $\sigma^* = Y\mathcal{H}/\ell_w$. The value of the maximum foot length possible before breakup is a function of σ_y/σ^* alone, shown graphically in Figure 4. Interestingly, we find that for sufficiently strong bergs, where $\sigma_y > 0.2012\sigma^*$, the buoyancy torque due to the foot is insufficient to cause the berg to break up, regardless of the length of the foot. This reflects the fact that for strong bergs, $\ell_{\text{crit}} \gg \ell_w$ and the foot actually adjusts to float at its natural buoyancy level.

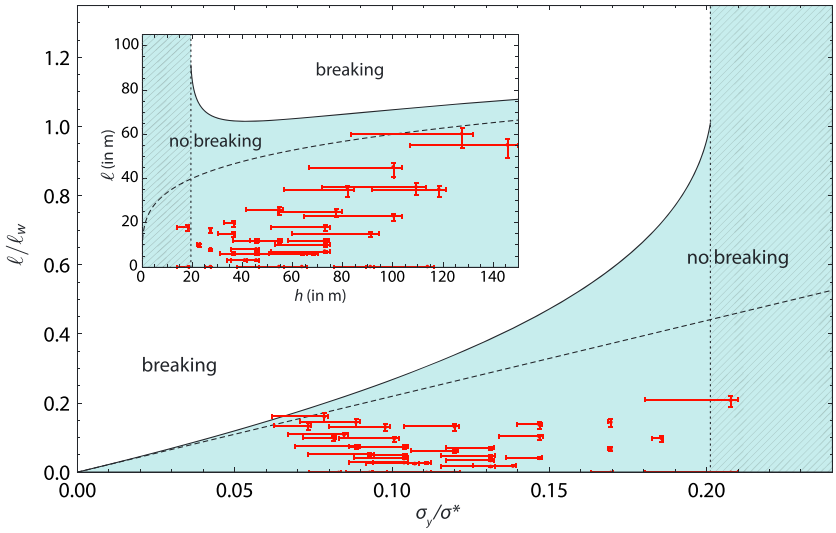

Figure 4. Regime diagram for dimensionless foot lengths against bending stress, shown are the exact solution for ℓ_{crit} (solid), the linear approximation (dashed), and the observational data (red points) from the PII-B-1 experiment; error bars are primarily due to the uncertainty in thickness measurements. The green shaded area represents the theoretical regime of $\ell(h)$ in which $\ell < \ell_{crit}$, i.e., where no breakup is expected from hydrostatic stresses. The hatched area shows the regime where $\sigma_{max} < \sigma_y$, for any ℓ. Inset: dimensional foot lengths ℓ versus iceberg thicknesses h.

4. Comparison With Observations

There are two features of our modeling approach that may readily be compared with experimental observation. The first is the theoretically predicted surface profile of an iceberg with a protruding ice foot, see equation (3). This may be compared with ICESat-based altimetric measurements of surface topography of Antarctic tabular icebergs [*Scambos et al.*, 2005]. In their study, the averaged line profiles of two large icebergs were given, with data reaching from the iceberg edge up to ∼3 km inward from the edge. These profiles exhibited what the authors call a rampart-moat shape—a raised edge, followed by a small depression away from the edge. *Scambos et al.* [2005] also presented the results of FEM calculations, which qualitatively recovered this characteristic profile. We note that the berg thicknesses and foot lengths reported there ($h = 250$ m, $\ell = 40$ m for A38B and $h = 200$ m, $\ell = 20$ m for A43B) with a Young's modulus of 0.1 GPa, giving $\ell_w = 345$ m and 292 m, respectively, correspond to a relatively small foot, i.e., $\ell/\ell_w \lesssim 0.1$. These simulations and experimental observations are therefore expected to lie in the "small foot" regime for which the beam profile is given by (3). As we see in Figure 3, this analytical prediction agrees well with both the observations and FEM results and, furthermore, indicates that this rampart-moat shape is universal once the horizontal and vertical dimensions have been rescaled as suggested in (3).

The second experimental observable that may be tested using the results of the model presented in section 3 is the length of the foot. Recall that the model predicts that if the foot reaches a critical length ℓ_{crit}, then the iceberg will fracture and a portion breaks off; in the field, therefore, we would expect to see feet with a wide range of lengths but all below this critical value. To compare the theory with our observations from PII-B-1, we segment the scan of the perimeter of the main iceberg into regions of similar edge/foot profiles and record both the approximate iceberg thickness and the foot length for each segment. The results obtained from this analysis are presented in dimensional form as the red dots in the inset of Figure 4. (To obtain these dimensional values, we take a medium value for the iceberg strength $\sigma_y = 500$ kPa [*Vaughan*, 1995; *Robe*, 1980] and $E = 1$ GPa [*Vaughan*, 1995].) An alternative way to present the data to highlight the role played by the yield stress σ_y is to plot the foot length as a function of σ_y/σ^*. This is done in the main portion of Figure 4. With both presentations of the data, we see that the experimental observations are consistent with theory in that for a given ice thickness, all observed feet appear to be shorter than some maximum length.

Considering Event 1, the average height of the broken-off piece was $h \approx 25$ m and length ≈100 m (Figure 2b). This compares well with the estimated point of maximum stress, $x_{max} \simeq 121$ m. The foot length

for this piece ℓ_{crit} varied widely from 0 to 28 m (average $\simeq$ 10 m) which compares to $\ell_{crit} \simeq 42$ m from the theory. The observed and predicted values can be brought to agreement by, for example, decreasing the assumed value for the yield stress. A mechanically weaker iceberg seems reasonable since the berg had already been drifting for 2 years by this point, and its surface was heavily crevassed. Indeed, taking $\sigma_y = 100$ kPa [*Van der Veen*, 1998] results in $\ell_{crit} \simeq 9$ m, thus consistent with our observations for Event 1. We hypothesize that any scenario in which the feet were longer than the maximum allowed would have caused breakup before our observations were made. We also note that for an iceberg of thickness $h = 50$ m, we find $\ell_{crit} \approx 50$ m, increasing to $\ell_{crit} \approx 72$ m for $h = 300$ m; $\ell_{crit} \sim h^{1/4}$ is only weakly dependent on the ice thickness. Furthermore, the small foot approximation is more accurate the thicker the berg (Figure 4, inset) and will be adequate for many Antarctic tabular icebergs, which often have thickness > 200 m.

5. Conclusions

Motivated by recent field observations, we have presented a quantitative model for an iceberg decay process that acts as a combination of melt and hydrostatic stress effects: we have argued that for icebergs floating in open water, rapid erosion near the water surface leads to a protruding underwater foot. The foot's upward buoyancy induces a stress field in the iceberg that can break off significant pieces from the edge of the berg. This model introduces a critical foot length ℓ_{crit} at which the iceberg will calve, for given material properties and berg thickness. For example, an Antarctic iceberg of thickness $h = 300$ m (and material values as above) will calve when the foot reaches $\ell_{crit} \approx 72$ m, resulting in the break off of a piece of $\sim$780 m length. In 5°C water, this foot length can be reached in as little as $\sim$2–3 weeks (assuming a differential erosion rate of 1 m/d/°C). This suggests that the footloose mechanism is a rapid and large-scale decay process for icebergs, and a significant contributor to their overall decay rate.

Acknowledgments

We are grateful to Max Fischer for technical support with the lidar and MB scanners and Markus Olsson for support with the GPS buoys. We would further like to thank Ian Eisenman for suggesting the name footloose mechanism, Anthony Anderson for helpful discussions, Jeremy Wilkinson for help in the early stages of the project, and Ted Scambos for insightful comments on an earlier version of the manuscript. We thank BBC Science for facilitating the field experiment. We are grateful to the Office of Naval Research High Latitude Program for supporting the University of Cambridge participation through the MIZ-DRI project, grant N00014-12-1-0130. T.J.W.W. further acknowledges ONR grant N00014-13-1-0469. The data used to produce the results of this letter are freely available upon request from the corresponding author.

The Editor thanks two anonymous reviewers for their assistance in evaluating this paper.

References

Alley, R. B. (2005), Ice-sheet and sea-level changes, *Science*, *310*(5747), 456–460.

Armstrong, T., B. Roberts, and C. Swithinbank (1973), *An Illustrated Glossary of Snow and Ice Terminology,* 2nd ed., Scott Polar Research Institute, Cambridge, U. K.

Derksen, C., et al. (2012), Variability and change in the Canadian cryosphere, *Clim. Change*, *115*(1), 59–88.

Diemand, D. (1987), On the splitting of icebergs: Natural and induced, *Proc. 6th Inter. Offshore Mech. and Arctic Eng. Symp.*, 1–9, Houston, Tex.

Falkner, K. K., H. Melling, and A. M. Münchow (2011), Context for the recent massive Petermann Glacier Calving Event, *Eos Trans. AGU*, *92*(14), 117.

Gladstone, R. M., G. R. Bigg, and K. W. Nicholls (2001), Iceberg trajectory modeling and meltwater injection in the Southern Ocean, *J. Geophys. Res.*, *106*(C9), 19,903–19,915.

Goodman, D. J., P. Wadhams, and V. A. Squire (1980), The flexural response of a tabular ice island to ocean swell, *Ann. Glaciol.*, *1*, 23–27.

Hetényi, M., and M. I. Hetbenyi (1946), *Beams on Elastic Foundation : Theory With Applications in the Fields of Civil and Mechanical Engineering*, Univ. of Michigan Press, Ann Arbor, Mich.

Huppert, H. E., and J. S. Turner (1978), On melting icebergs, *Nature*, *271*, 46–48.

Keghouche, I., and L. Bertino (2009), Parameterization of an iceberg drift model in the Barents Sea, *J. Atmos. Oceanic Technol.*, *26*(10), 2216–2227.

Landau, L. D., and E. M. Lifshitz (1986), *Theory of Elasticity*, Pergamon Press, Oxford, U. K.

Mansfield, E. H. (2005), *The Bending and Stretching of Plates*, Cambridge Univ. Press, Cambridge, U. K.

Martin, S., R. Drucker, R. Aster, F. Davey, E. Okal, T. Scambos, and D. MacAyeal (2010), Kinematic and seismic analysis of giant tabular iceberg breakup at Cape Adare, Antarctica, *J. Geophys. Res.*, *115*, B06311, doi:10.1029/2009JB006700.

McClintock, J. B. (2011), Arctic: Sea-ice loss sparks oil drilling boom, *Nature*, *479*(7374), 478.

Padman, L., and S. Erofeeva (2004), A barotropic inverse tidal model for the Arctic Ocean, *Geophys. Res. Lett.*, *31*, L02303, doi:10.1029/2003GL019003.

Rignot, E., G. Casassa, P. Gogineni, W. Krabill, A. Rivera, and R. Thomas (2004), Accelerated ice discharge from the Antarctic Peninsula following the collapse of Larsen B ice shelf, *Geophys. Res. Lett.*, *31*, L18401, doi:10.1029/2004GL020697.

Robe, R. Q. (1980), Iceberg drift and deterioration, in *Dynamics of Snow and Ice Masses*, edited by S. C. Colbeck, pp. 211–258, Academic, Press, New York.

Savage, S. B. (2001), *Aspects of Iceberg Deterioration and Drift*, pp. 279–318, Springer, Berlin, Heidelberg, Germany.

Scambos, T., O. Sergienko, A. Sargent, D. MacAyeal, and J. Fastook (2005), ICESat profiles of tabular iceberg margins and iceberg breakup at low latitudes, *Geophys. Res. Lett.*, *32*, L23S09, doi:10.1029/2005GL023802.

Scambos, T., R. Ross, R. Bauer, Y. Yermolin, P. Skvarca, D. Long, J. Bohlander, and T. Haran (2008), Calving and ice-shelf break-up processes investigated by proxy: Antarctic tabular iceberg evolution during northward drift, *J. Glaciol.*, *54*(187), 579–591.

Sierro, F. J., et al. (2005), Impact of iceberg melting on Mediterranean thermohaline circulation during Heinrich events, *Paleoceanography*, *20*, PA2019, doi:10.1029/2004PA001051.

Silva, T., G. R. Bigg, and K. W. Nicholls (2006), Contribution of giant icebergs to the Southern Ocean freshwater flux, *J. Geophys. Res.*, *111*, C03004, doi:10.1029/2004JC002843.

Smith, L. C., and S. R. Stephenson (2013), New trans-Arctic shipping routes navigable by midcentury, *Proc. Natl. Acad. Sci. U.S.A.*, *110*(13), E1191–E1195.

Timco, G. (2007), Grand Banks iceberg management, *Tech. Rep. 20–84*, PERD/CHC, National Research Council Canada, Ottawa, Ont., Canada.
Van der Veen, C. (1998), Fracture mechanics approach to penetration of bottom crevasses on glaciers, *Cold Reg. Sci. Technol.*, *27*(3), 213–223.
Vaughan, D. G. (1995), Tidal flexure at ice shelf margins, *J. Geophys. Res.*, *100*(B4), 6213–6224.
Veitch, B., M. Williams, A. Gardner, and B. Liang (2001), Field observations of iceberg deterioration, *Tech. Rep. 20–64*, PERD/CHC, National Research Council Canada, Ottawa, Ont., Canada.
Vella, D., and J. S. Wettlaufer (2008), Explaining the patterns formed by ice floe interactions, *J. Geophys. Res.*, *113*, C11011, doi:10.1029/2008JC004781.
Wadhams, P. (2000), *Ice in the Ocean*, Gordon and Breach Science Publishers, London, U. K.
Wadhams, P., M. Kristensen, and O. Orheim (1983), The response of Antarctic icebergs to ocean waves, *J. Geophys. Res.*, *88*(C10), 6053–6065.
Wagner, T. J. W., and D. Vella (2011), Floating carpets and the delamination of elastic sheets, *Phys. Rev. Lett.*, *107*, 044301.
White, F. M., M. L. Spaulding, and L. Gominho (1980), Theoretical estimates of the various mechanisms involved in iceberg deterioration in the open ocean environment, *Tech. Rep. USCG-D-62-80*, Rhode Island University, Kingston, R. I.
World Meteorological Organization (1970), World Meteorological Society sea-ice nomenclature, *WMO/OMM/BMO, Publ. 259*, 147, World Meteorological Society, Geneva, Switzerland.